frontiers | Frontiers in Energy Research

ORIGINAL RESEARCH
published: 08 June 2022
doi: 10.3389/fenrg.2022.878747

Preparation and Thermophysical Properties of Sodium Nitrate/Nanoparticle/Expanded Graphite Composite Heat Storage Material

Wenbing Song, Yuanwei Lu, Zhansheng Fan and Yuting Wu*

MOE Key Laboratory of Enhanced Heat Transfer and Energy Conservation, Beijing Key Laboratory of Heat Transfer and Energy Conversion, Faculty of Environment and Life, Beijing University of Technology, Beijing, China

As a medium and high temperature heat storage medium, the thermal performance of molten salt plays an important role in the thermal energy storage system. In order to improve the specific heat capacity and thermal conductivity of molten salt, a mechanical dispersion method is used to prepare a shape-stable composite phase change material for thermal energy storage. Nitrate ($NaNO_3$) has a higher phase change latent heat, which was chosen to combined with different nanoparticles (SiO_2, SiO_2+TiO_2) to improve its specific heat capacity, and with expanded graphite (EG) as a carrier matrix to improve thermal conductivity. Through the characterization of its chemical compatibility and thermophysical properties, the results show that the nanoparticles, EG and $NaNO_3$ have good chemical compatibility. Compared to $NaNO_3$, the thermophysical properties of composite ($NaNO_3$:(SiO_2+TiO_2):EG = 84%:0.1% + 0.9%:15%, mass ratio) was improved obviously. The average specific heat capacity before the phase change increased from 1.45 J/(g·K) to 1.81 J/(g·K), and the average specific heat capacity after the phase change increased from 1.69 J/(g·K) to 2.47 J/(g·K); The thermal conductivity is about 13.9 times higher than that of $NaNO_3$; in the range of 100–380°C, the heat storage density of the composites is about 679.2 kJ/kg 300 thermal stability tests showed that the latent heat of the composites is reduced by 7.4%, and the specific heat capacity before and after the phase change is reduced by 6.1 and 6.0%, respectively. The research can provide a broad application prospects in the field of medium temperature energy storage.

Keywords: molten salt, expanded graphite, nanoparticle, composite material, thermophysical properties

OPEN ACCESS

Edited by:
Yi-Lin Wu,
Cardiff University, United Kingdom

Reviewed by:
Xianglei Liu,
Nanjing University of Aeronautics and Astronautics, China
Xiangfei Kong,
Hebei University of Technology, China

****Correspondence:***
Yuanwei Lu
luyuanwei@bjut.edu.cn

Specialty section:
This article was submitted to Solar Energy, a section of the journal Frontiers in Energy Research

Received: *18 February 2022*
Accepted: *26 April 2022*
Published: *08 June 2022*

Citation:
Song W, Lu Y, Fan Z and Wu Y (2022) Preparation and Thermophysical Properties of Sodium Nitrate/Nanoparticle/Expanded Graphite Composite Heat Storage Material. Front. Energy Res. 10:878747. doi: 10.3389/fenrg.2022.878747

INTRODUCTION

In the end use of energy, more than 50% exists in the form of heat energy. How to use thermal energy storage (TES) technology to make full use of discontinuous and unstable heat, such as solar heat utilization (Ju et al., 2017)and industrial waste heat (Yang et al., 2018), has become an important environmental protection technology to improve energy efficiency. Thermal energy storage includes sensible heat storage, latent heat storage and thermochemical heat storage (Song et al., 2018a). At present, thermochemical heat storage is still in the laboratory-scale basic research, while sensible heat storage has been widely used in practical applications. However, sensible heat storage still suffers from the problem of low energy storage density. Compared with sensible heat storage technology, latent heat storage using phase change materials (PCM) has

high energy storage density, and heat is stored/released in a smaller temperature range, so latent heat storage is considered as a very promising TES technology (Da Cunha and Eames, 2016; Gasia et al., 2016).

PCMs are divided into organic and inorganic (Kim et al., 2016). Organic PCMs include paraffin (Li et al., 2014; Ling et al., 2015), alkanes (Kim et al., 2016), fatty acids (Wen et al., 2016), polymers (Mu et al., 2016a; Liu et al., 2016) and their mixtures (Mu et al., 2016b; Wei et al., 2016), which are mainly used to store low-temperature heat with T < 120°C. Inorganic PCM mainly includes hydrated salt (mainly used for T < 120°C), nitrate (Li et al., 2016), carbonate (Tao et al., 2015), chloride (Tian et al., 2016), sulfate (Qin et al., 2015) and metals, which can be used for medium and high temperature (200–1,400°C) (Xiao et al., 2014; Zhong et al., 2014; Tian et al., 2015). Recently, nitrates are widely used as TES materials in solar applications such as concentrating solar power (CSP) because of its low melting point, low causticity, high thermal stability and reasonable commercial price (Farid et al., 2004). Sodium nitrate seems to be a good material for the latent heat storage. Its latent heat is relatively high. Moreover, it is a single component with a high commercial availability and is easier to manufacture than eutectic salt. However, molten sodium nitrate is a solid-liquid phase change material, and it is necessary to prevent leakage during the solid-liquid phase change process. At the same time, poor thermal conductivity and small specific heat capacity also limit its heat storage performance (Zhuo and Wu, 2014; Fernández et al., 2015; Gimenez and Fereres, 2015).

At present, one method to improve the low thermal conductivity and avoid the leakage of liquid phase is to develop shape-stable PCM (SSPCM) composites (Zalba et al., 2003; Qiao et al., 2021). Inorganic materials with a large surface area and a microporous structure are selected as the carrier material, and the liquid molten salt is inhaled into the micropores through the capillary force of the micropores to form a composite heat storage material (Liu et al., 2015; Tao et al., 2020), which can not only improve the thermal conductivity of the material, it can also reduce the leakage of molten salt (Zhang et al., 2015). Expanded graphite (EG) has the advantages of high thermal conductivity, large specific surface area, loose pores, low density, good dispersibility, and good corrosion resistance, so it is often selected as a carrier material (Wang et al., 2009). Acem (Acem et al., 2010; Lopez et al., 2010) prepared KNO_3-$NaNO_3$/EG composite phase change materials, and found that the thermal conductivity of the composites can be increased by 20 times when the addition amount of EG is 20 wt%. Ren (Ren et al., 2018) prepared $Ca(NO_3)_2$-$NaNO_3$/EG composite phase change material and found that the thermal conductivity of the composites containing 7 wt% EG can be improved by 7.3 times higher than that of pure binary salt. Yu (Yu et al., 2020) prepared KNO_3-$NaNO_3$/SiO_2/EG composite material, and found that the thermal conductivity of the composites added with 15 wt% EG and 1.0 wt% SiO_2 nanoparticles is increased by 16.2 times. The above results show that different methods combined with EG can significantly improve the thermal conductivity of molten salt.

In addition, the specific heat of molten salt is very important for the storage of heat energy. Related studies have shown that adding nanoparticles (Nano) to molten salt can increase the specific heat capacity of molten salt (Shin and Banerjee, 2011; Tiznobaik et al., 2015; Madathil et al., 2016). Andreucabedo (Andreu-Cabedo et al., 2014) added SiO_2 nanoparticles with mass fraction of 0.5, 1.0, 1.5 and 2.0 wt% to solar salt. When the mass fraction of SiO_2 was 1.0%, the specific heat could be increased by 25%. Manila (Chieruzzi et al., 2013) added SiO_2, Al_2O_3, TiO_2 and SiO_2-Al_2O_3 nanoparticles to solar salt respectively, and studied the effects of three mass fractions (0.5, 1.0 and 1.5 wt%) on the thermophysical properties of molten salt. The results show that when the mass fraction of each kind of nanoparticles is 1 wt%, the specific heat is improved the most. In particular, the addition of SiO_2-Al_2O_3 nanoparticles has the largest increase in specific heat, with a 57% increase in the solid phase and 22% increase in the liquid phase. The author's team also found that when 20 nm, 0.1 wt%SiO_2+0.9 wt%TiO_2 nanoparticles are added to quaternary nitrate, the specific heat increase is greater than when SiO_2 or TiO_2 is added alone (Yu et al., 2021). The above research shows that the addition of nanoparticles can effectively improve the specific heat capacity of molten salt, and the effect of adding two kinds of nanoparticles at the same time is better than adding one kind of nanoparticles alone. However, the defect of adding nanoparticles is that nanoparticles will reunite during long-time standing. If the nanoparticle-added molten salt is combined with EG, the molten salt nanofluid can be adsorbed in the pores of EG, which can not only avoid the agglomeration of nanoparticles in the molten salt, but also improve its thermal conductivity and specific heat (Yu et al., 2020). In addition, combining molten salt with nanoparticles and EG to form a shape-stable heat storage material, while utilizing its latent and sensible heat, the heat storage density is greatly improved. However, there is still a lack of research on the influence of molten salt with different kinds of nanoparticles combined with EG on the thermophysical properties of molten salt.

Therefore, in this paper, $NaNO_3$ was selected as the phase change material, two different nanoparticles (1.0 wt% SiO_2, 0.1 wt % SiO_2 + 0.9 wt% TiO_2) were added to $NaNO_3$, and EG was used as the carrier matrix, the $NaNO_3$/Nano/EG composites is prepared by mechanical dispersion method. Then, its chemical compatibility and micro structure were characterized by X-ray diffraction (XRD) and scanning electron microscopy (SEM). The thermal performance of $NaNO_3$/Nano/EG composites was investigated using differential scanning calorimeter (DSC), Laser flasher (LFA). In addition, the stability of the $NaNO_3$/(SiO_2+TiO_2)/EG composite was verified by thermal stability test.

MATERIALS AND METHOD

Materials

Sodium nitrate (AR, purity >99%) was purchased from Beijing Tong guang fine chemical company. Silica nanoparticles (average diameter 20 nm, specific surface area 200 m^2/g, spherical, purity>99%), titanium dioxide nanoparticles (average diameter

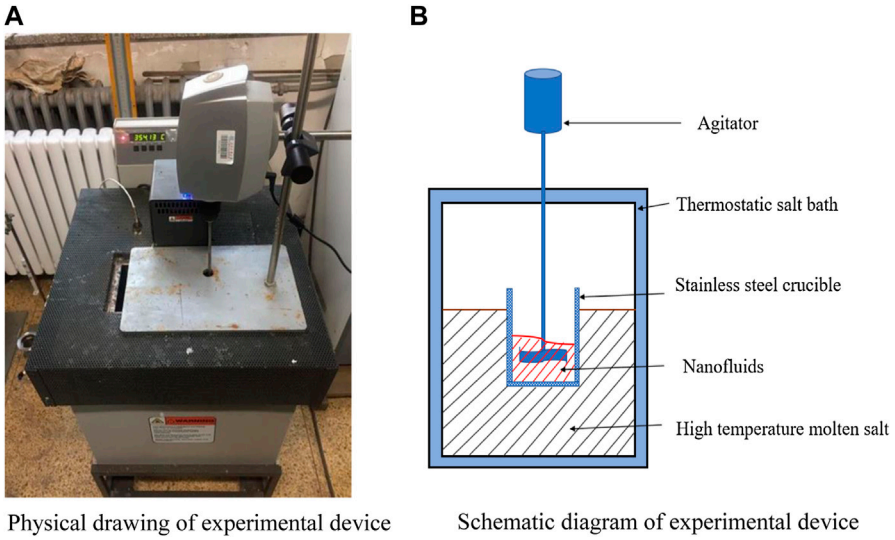

FIGURE 1 | Experimental picture and schematic diagram for the nanofluid preparation. **(A)** Physical drawing of experimental device. **(B)** Schematic diagram of experimental device.

20 nm, specific surface area 30–50 m^2/g, spherical, purity>99%) and expandable graphite powder purchased from Beijing Deke Dao jin Science and Technology Co., Ltd. The expandable volume of expanded graphite powder is 300 ml/g and the particle size is 80 mesh. Using expandable graphite powder as raw material, EG is prepared by microwave method.

Preparation and Optimization of Composite Materials

Preparation of Nanofluids

Weigh a certain amount of sodium nitrate and silica nanoparticles, and stir them with a mechanical stirrer in a constant temperature salt bath at 400°C. The stirring speed is 750 r/min, and the stirring time is 15 min (Song et al., 2018b). Finally, a molten salt nanofluid with a mass fraction of SiO_2 of 1 wt% is obtained. The physical drawing and schematic diagram of mechanical mixing device are shown in **Figure 1**. The molten salt nanofluid with SiO_2 mass fraction of 0.1 wt% and TiO_2 mass fraction of 0.9 wt% was prepared by the same method.

Preparation of Composite Materials

The prepared $NaNO_3/SiO_2$ molten salt nanofluid was placed in a 400°C constant temperature salt bath, and different mass fractions (7, 10, 15, 20 wt%) of EG were added.

Stir with a stir bar until the liquid molten salt completely enters the pores of the EG, and the stirring time is about 60 min; take the mixture out, cool and grind in a desiccator, and then the powdered $NaNO_3/SiO_2$/EG composite material can be obtained.

The powder is pressed into a shape with a pressing machine, the molding pressure is 10 MPa, and the pressure holding time is 60 s (Yu et al., 2020), to form a cylindrical sample with a diameter of 12.5 mm and a height of 2.5 mm. Put the pressed sample into a muffle furnace for sintering. During sintering, the heating rate between 30–150°C was 2°C/min (the slow heating rate was to make a small amount of water in the original sample evaporate completely); the heating rate is 5 °C/min between 150 and 400°C, keep the temperature at 400°C for 90 min to make the composite material fully adsorb and mix (Ren et al., 2018; Yu et al., 2020). The sample was naturally cooled to room temperature, and a sintered $NaNO_3/SiO_2$/EG composite material was obtained. The process of preparing samples by mechanical dispersion method is shown in **Figure 2**.

Optimization of Composite Materials

In order to explore the optimal addition amount of EG, the prepared samples were characterized by morphology and mass analysis before and after sintering. In this study, the composite phase change materials with basically unchanged appearance before and after sintering and high adsorption degree of EG to molten salt need to be selected to determine the optimal addition amount of EG. The sintered appearance of the composite material with different mass fractions of EG is shown in **Figure 3**. The mass changes of composites before and after sintering are shown in **Table 1**.

Combining **Figure 3** and **Table 1**, it is found that the composite material sample with 7 wt% EG has a serious leakage, and the mass loss rate is as high as 18.19%. The mass loss rate of the composite material with 10 wt% EG is 11.03%, there are many small pits on the surface of the sample, which is not enough smooth. The mass loss rate of the composites with 15 wt% EG and 20 wt% EG added is less than 5%, and the sample surface is smooth and flat. Therefore, this study determined that the optimal addition amount of EG was 15 wt%. Using the same method, $NaNO_3/(SiO_2+TiO_2)$/EG composite material was prepared. The addition ratios of SiO_2 nanoparticles, TiO_2 nanoparticles and EG were 0.1, 0.9, and 15 wt%, respectively. In order to explore

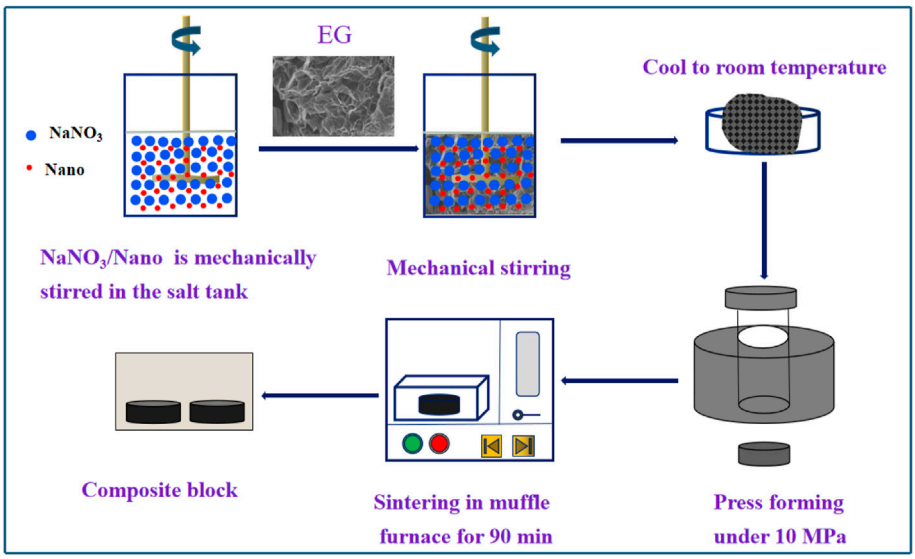

FIGURE 2 | The composite preparation process with mechanical dispersion method.

FIGURE 3 | Morphology of composites with different EG content after sintering.

TABLE 1 | mass loss rate of composites with different EG content.

EG (wt%)	Mass before sintering (g)	Mass after sintering (g)	Mass loss rate
7	0.5633	0.4608	18.19%
10	0.7274	0.6472	11.03%
15	0.4049	0.3886	4.03%
20	0.3964	0.3883	2.04%

TABLE 2 | composition of different samples.

Sample	Molten salt	EG (wt%)	SiO_2(wt%)	TiO_2(wt%)
1	$NaNO_3$	—	—	—
2	$NaNO_3$	—	1	—
3	$NaNO_3$	—	0.1	0.9
4	$NaNO_3$	15	—	—
5	$NaNO_3$	15	1	—
6	$NaNO_3$	15	0.1	0.9

the effect of adding nanoparticles and eg on the thermophysical properties of sodium nitrate, the comparison samples shown in **Table 2** were prepared in this paper.

Characterization

SEM-EDS and XRD

The microstructures and elemental analysis for the composite materials were characterized by scanning electron microscopy (SEM, ZEISS Gemini 300) and energy dispersive spectrometry (EDS). The sample is dried in a drying oven to prevent the effect of small amount of moisture inhaled in the sample on the characterization results. Due to the poor conductivity of the molten salt itself, it is necessary to spray gold on the dried samples to improve the conductivity of the samples.

The composites were characterized by X-ray diffractometer (XRD, D8-ADVANCE, BRUKER/AXS, Germany) to determine its chemical composition, crystal structure and other information of the sample. The diffractometer uses Cu target, the scanning range is 20^{o}-80^{o}.

Characterization of Phase Transition Characteristics and Specific Heat Capacity

The specific heat, latent heat and the phase change temperature of the sample were measured by a synchronous thermal analyzer (STA-449F3, NETZSCH). The sample was sealed in an aluminum crucible. In order to ensure uniform heat transfer between the crucible and the sample, the sample mass and heat ramp rate should be controlled at

5–15 mg and 10 K/min, respectively, with a nitrogen atmosphere with a nitrogen flow rate of 50 ml/min. The sample was kept at a constant temperature of 30°C for 10 min, and then heated from 30 to 400°C at a heating rate of 10 K/min, and kept at 400°C for 10 min. The extrapolated starting temperature on the differential scanning calorimetry (DSC) curve is selected as the melting temperature of the sample. This temperature can be determined by the intersection of the extension of the baseline and the tangent to the initial linear portion of the peak. The latent heat of phase change is calculated by integrating the area under the peak of the DSC curve. In the determination of specific heat capacity, sapphire is usually used as a standard material, and its data has been accurately determined. By comparing the measured values of the standard sample (sapphire) with known specific heat and the sample to be tested, the specific heat capacity of the sample to be tested can be obtained.

In order to further ensure the reliability of the results, each sample in the experiment was measured at least three times, and the following equation was used to calculate the standard deviation of the measurement results.

$$S = \sqrt{\frac{\sum_{i=1}^{n} (X_i - \bar{X})^2}{n-1}} \tag{1}$$

where, S is the standard deviation of the sample; X_i is the measured value of the sample; $\bar{X}$ is the average of three measurements.

The heat storage density of composites can be calculated by **Formula (2)**.

$$\begin{aligned} Q_m &= \int_{T_s}^{T_m} mc_p dT + m\Delta H + \int_{T_m}^{T_1} mc_p dT \\ &= mc_p (T_m - T_s) + m\Delta H + mc_p (T_1 - T_m) \end{aligned} \tag{2}$$

Where, Q_m means heat storage density (kJ/kg), m means mass (kg), c_p means specific heat (J/(gK)), T_m means melting temperature (°C), T_s means initial temperature (°C), T_1 represents the termination temperature (°C), ΔH represents the latent heat (J/g).

Characterization of Thermal Conductivity

Thermal diffusivity of the composites was characterized by a laser thermal conductivity meter (LFA-45, NETZSCH). During the measurement, the laser pulse is emitted to the bottom of the sample through the laser beam, and after absorbing the light energy, the temperature of the bottom surface of the sample rises instantly. Suppose the heat conduction is one-dimensional, and the heat is transferred to the top surface. The temperature change of the center of the top surface of the sample is measured continuously by infrared sensor above the sample. The thermal diffusivity along the thickness of the sample can be obtained by increasing the surface temperature of the sample. The thermal diffusivity (α) can be calculated by **Formula (3)**.

$$\alpha = \frac{d^2}{t_{1/2}} \tag{3}$$

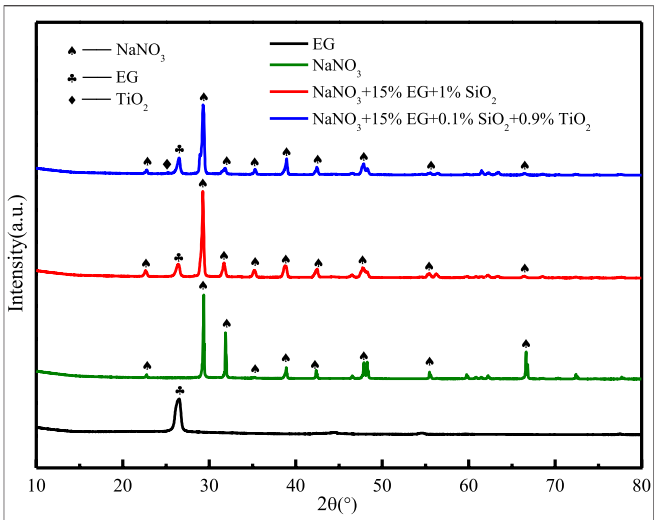

FIGURE 4 | XRD patterns of EG, $NaNO_3$ and its composites.

Where, α represents the thermal diffusivity (mm^2/s), d represents the sample thickness (mm), and $t_{1/2}$ is the time for the maximum temperature to rise by 50% (s).

According to **Formula (4)**, the thermal conductivity can be calculated.

$$\lambda = \alpha \cdot \rho \cdot c_p \tag{4}$$

Where, λ represents the thermal conductivity (W/(mK)), ρ is the density (g/m^3) (Calculated based on the mass of the weighed composite material and the measured volume), α is the thermal diffusivity (mm^2/s), c_p is the specific heat (J/(gK)).

Thermal Stability Test

The thermal cycle stability of the composites was tested in a high temperature muffle furnace. The corundum crucible containing the sample was put into a muffle furnace, which was heated from room temperature to 400°C at the heating ramp rate of 10 K/min to complete the phase transformation endothermic process, and keep constant temperature at 400°C for 10 min, then cooled to room temperature to complete the exothermic process. This cycle is repeated 100 times.

RESULTS AND DISCUSSION

Chemical Compatibility of Composite Materials

Figure 4 shows the XRD diffraction pattern of EG, $NaNO_3$, $NaNO_3/SiO_2$/EG and $NaNO_3/(SiO_2+TiO_2)$/EG composite materials for chemical compatibility analysis. It can be seen that there are only three peaks of $NaNO_3$, EG and TiO_2 in the XRD spectrum, and all the peaks are in one-to-one correspondence, indicating that no other new substances are formed. SiO_2 is amorphous, so no SiO_2 peak is observed on the XRD spectrum, and the content of TiO_2 is very few, so its diffraction peak is also particularly small. At the positions of $2\theta = 32^o$ and $2\theta = 67^o$, the intensity of the $NaNO_3$ diffraction peaks in

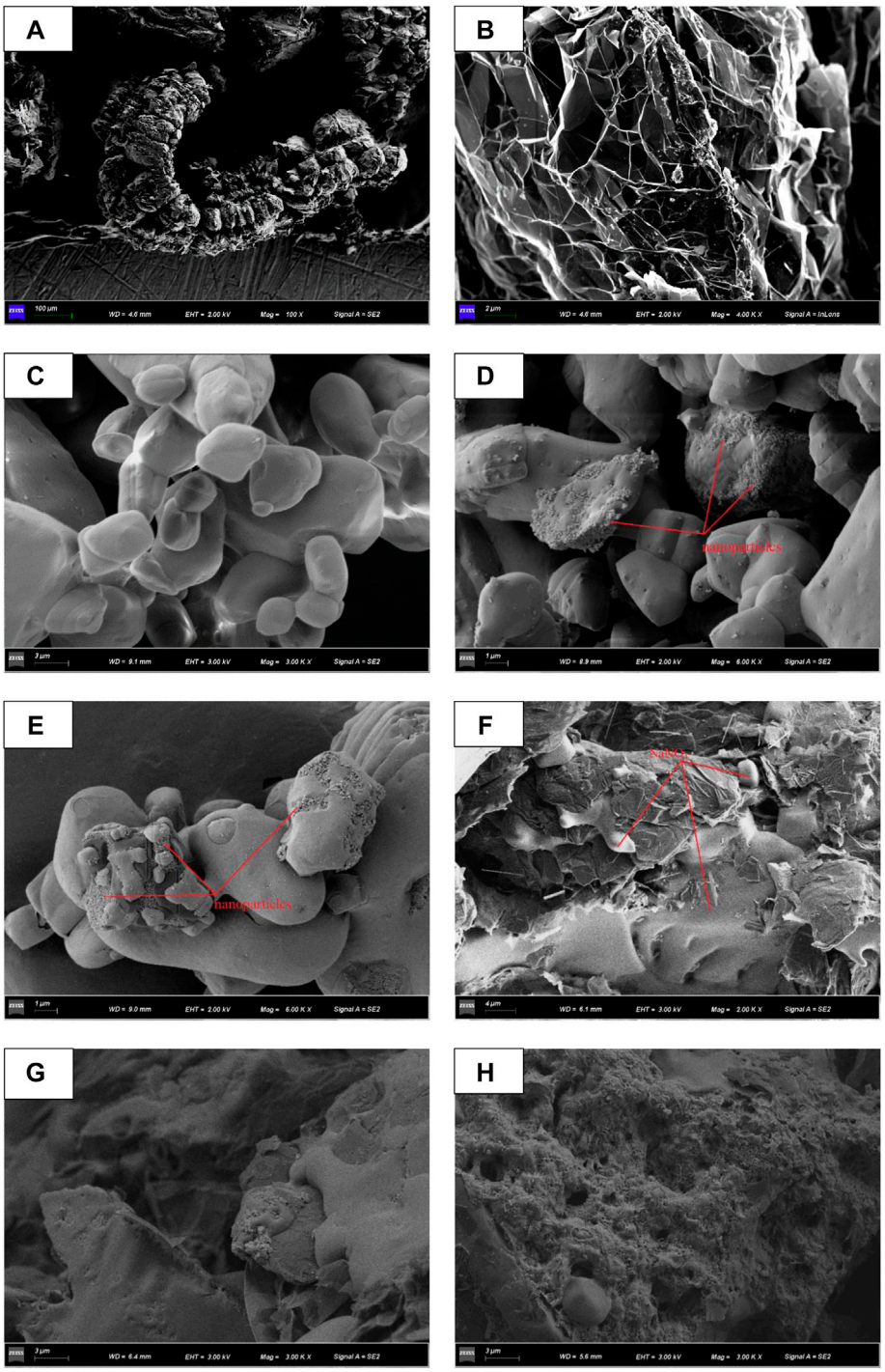

FIGURE 5 | SEM image **(A, B)** EG, **(C)** $NaNO_3$, **(D)** $NaNO_3/SiO_2$, **(E)** $NaNO_3/(SiO_2+TiO_2)$. **(F)** $NaNO_3$/EG, **(G)** $NaNO_3/SiO_2$/EG, **(H)** $NaNO_3/(SiO_2+TiO_2)$/EG.

the composite materials is observed to be reduced, which may be related to the influence of compression and sintering on the crystal structure of the composites and the volatilization of a small amount of nitrate. To sum up, the composites are only a physical mixture of $NaNO_3$, EG and nanoparticles, and there is no chemical reaction between them.

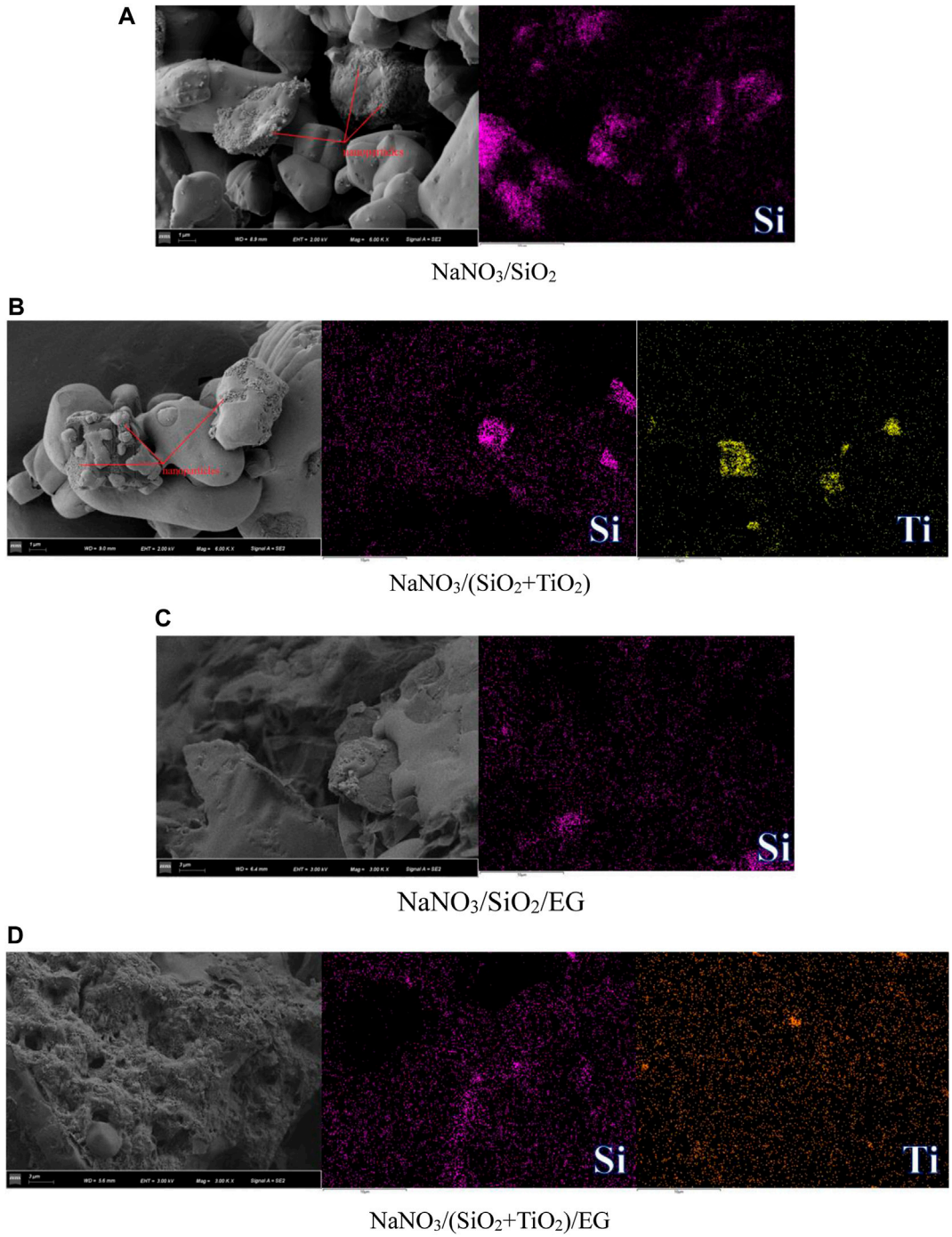

FIGURE 6 | EDS element mapping images of different samples. **(A)** NaNO3/SiO2. **(B)** $NaNO_3/(SiO_2+TiO_2)$. **(C)** $NaNO_3/SiO_2/EG$. **(D)** $NaNO_3/(SiO_2+TiO_2)/EG$.

Microstructure Characterization and Element Distribution of Composites

Figure 5 shows the microstructure images of different samples by a scanning electron microscope. **Figure 5A** shows that EG is a wormlike structure at ×100 magnification, and **Figure 5B** shows that EG contains abundant cellular network structure at ×4,000 magnification, which can provide enough pores for adsorption of molten salt. **Figure 5C** shows that $NaNO_3$ exhibits a crystal block structure of different sizes due to its uneven particle size. **Figures 5D,E** are SEM images of $NaNO_3/SiO_2$ and $NaNO_3/(SiO_2+TiO_2)$ composites, respectively. In the high-magnification SEM image, it can be clearly seen that the nanoparticles are attached to the

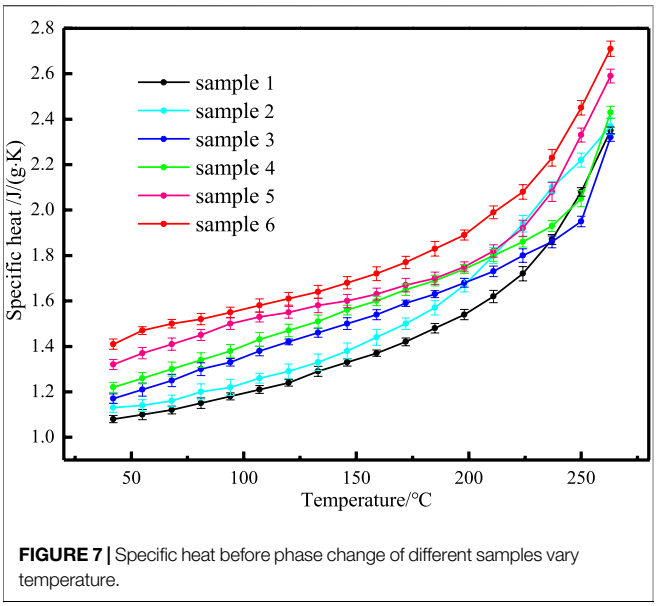

FIGURE 7 | Specific heat before phase change of different samples vary temperature.

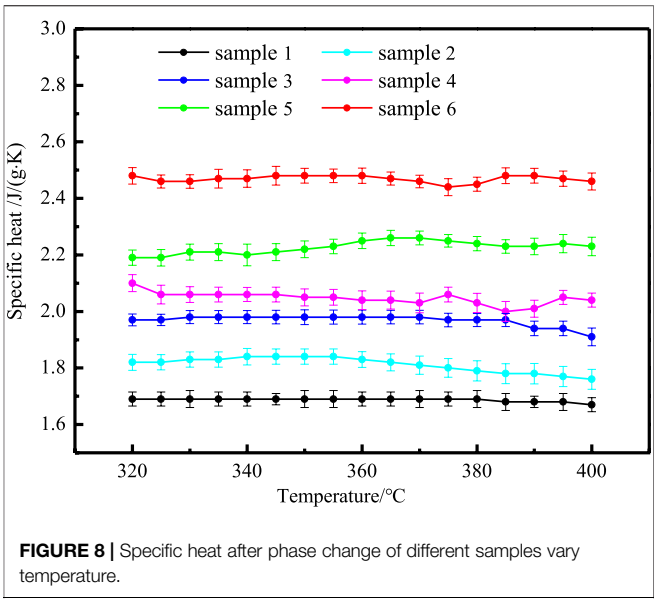

FIGURE 8 | Specific heat after phase change of different samples vary temperature.

surface of $NaNO_3$, forming a nanostructure with a larger specific surface area and surface energy.

Figures 5F–H, are the images obtained by cutting the sample along the center line to observe the cross section. **Figure 5F** is the SEM image of the $NaNO_3$/EG composite material. EG provides many porous structures. It can be observed that $NaNO_3$ is embedded in the pores of EG to ensure that it does not leak during phase change. **Figures 5G,H** are SEM images of $NaNO_3/SiO_2$/EG and $NaNO_3/(SiO_2+TiO_2)$/EG composites respectively. It can be seen that $NaNO_3$ is adsorbed in the porous structure of EG, partly between the surface layers of EG, and nanoparticles are attached to the surface of $NaNO_3$ and EG, forming a dense network of nanostructures.

In order to further observe the distribution of nanoparticles in the composite material, EDS element mapping was performed on the area where the SEM images of different samples were located. As shown in **Figure 6A**, the distribution of Si element in $NaNO_3/SiO_2$ composite is basically uniform, and local agglomeration occurs in some areas, in this area, the content of Si element is 0.23wt%. As shown in **Figure 6B**, the distribution of Si and Ti elements in $NaNO_3/(SiO_2+TiO_2)$ composites is uniform in most areas, but obvious agglomeration occurs in a small part of the area. In the whole area, the contents of Si and Ti elements are respectively is 0.03wt% and 0.11 wt%. As shown in **Figure 6C**, the distribution of Si element in the $NaNO_3/SiO_2$/EG composite is very uniform in the whole area, in this area, the content of Si element is 0.3 wt%. As shown in **Figure 6D**, the distribution of Si and Ti elements in $NaNO_3/(SiO_2+TiO_2)$/EG composites is uniform in whole areas, and the contents of Si and Ti elements are respectively is 0.06wt% and 0.17 wt%. In summary, it can be seen that if only nanoparticles are added to $NaNO_3$, the nanoparticles will be unevenly dispersed and agglomerated. However, by adsorbing the $NaNO_3$ added with nanoparticles in the pores of EG, the agglomeration of nanoparticles can be effectively prevented, and the dispersion of nanoparticles can be more uniform.

Thermophysical Properties of Samples

Specific Heat of Samples

The phase change process of composites with temperature includes three stages: solid state, phase change process and liquid state. The specific heat of different samples before phase transition is shown in **Figure 7**, which increases with the increase of temperature. The specific heat of different samples before phase transition is shown in **Figure 8**, which remains basically unchanged with the increase of temperature. The standard deviation of specific heat capacity of all samples is less than 4%. **Table 3** shows the average specific heat capacity of different samples in different temperature ranges according to the measurement curve.

It can be seen from **Table 3** that adding nanoparticles and EG alone improves the specific heat of sodium nitrate, and the influence of adding two kinds of nanoparticles is better than adding one kind of nanoparticles. In addition, when adding nanoparticles and EG at the same time, the increase in specific heat is significantly greater than adding nanoparticles or EG alone.

The specific heat of molten salt can be increased by adding nanoparticles, because nanoparticles adhere to the surface of molten salt to form semi-solid nanolayer. This kind of semi-solid nanolayer has higher thermal performance than liquid, which helps to increase the specific heat of nanofluid (Shin and Banerjee, 2011; Lu and Huang, 2013). It can be seen from the above SEM image that after adding SiO_2 (SiO_2+TiO_2) nanoparticles to $NaNO_3$, a dense solid-like nanostructure is also formed. This structure has a large specific surface area and specific surface energy, thereby increasing the specific heat capacity of the composites. When Shin (Shin and Banerjee, 2014) studied pure molten salt nanofluid, it was also found that similar structures appeared on the surface. Luo et al. (Luo et al., 2022) proposed a 3D hierarchical ultralight SiC foam with 1 wt% SiO_2 added $LiNO_3$/NaCl inside to achieve high specific heat capacity. The average c_p is 4.86% higher than that of pure PCMs due to the

TABLE 3 | The specific heat of different samples.

Samples	Component	The average specific heat (40–265°C) (J/(g·K))	The average specific heat (320–400°C) (J/(g·K))
Sample 1	$NaNO_3$	1.45	1.69
Sample 2	$NaNO_3/SiO_2$	1.54	1.81
Sample 3	$NaNO_3/(SiO_2+TiO_2)$	1.56	1.97
Sample 4	$NaNO_3$/EG	1.62	2.05
Sample 5	$NaNO_3/SiO_2$/EG	1.71	2.23
Sample 6	$NaNO_3/(SiO_2+TiO_2)$/EG	1.81	2.47

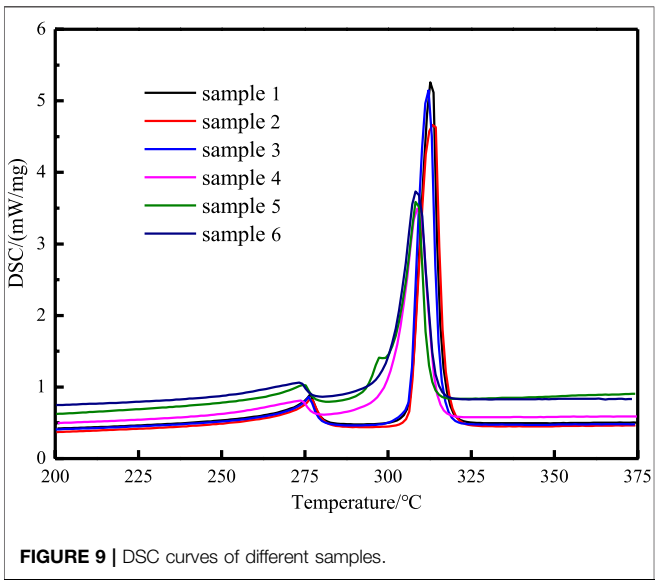

FIGURE 9 | DSC curves of different samples.

high surface energy and interfacial thermal resistance induced by weak interaction between SiO_2 nano-particles and eutectics, as confirmed by molecular dynamics (MD) simulations.

The addition of EG can increase the specific heat of sodium nitrate. This is because the mechanical energy of $NaNO_3$ and EG is converted into the interface energy of the composite by the tablet press in the process of preparing the composite. The increase of the interface energy may promote the specific heat of the composites.

After adding nanoparticles and EG at the same time, the nanoparticles adhere to the surface of molten salt and EG, forming a dense network of nanostructures, and because the molten salt is adsorbed by porous structure of EG, it overcomes the phenomenon that the nanoparticles are not uniformly dispersed in the molten salt and agglomeration occurs in the process of long standing. Therefor the nanoparticles more uniformly dispersed in the composites. The synergy between nanoparticles and EG can greatly increase the specific heat capacity of the composites. In addition, on the basis of adding EG, the influence of adding (SiO_2+TiO_2) nanoparticles is better than adding only SiO_2 nanoparticles. This may be because molten salt and EG have different forces on SiO_2 and TiO_2 molecules. Therefore, when nanostructures are generated, the nanostructures generated by the former are more uniform and continuous in the composites than the latter, which in turn affects the specific heat of the composites.

Phase Change Characteristics and Heat Storage Density of Samples

The phase change temperature and latent heat have an important influence on the heat storage performance of the composite phase change material. **Figure 9** shows the DSC curves of different samples. The thermophysical parameters obtained according to the curve analysis are listed in **Table 4**. It can be seen from the DSC curve that there is a solid-solid phase change peak of sodium nitrate at about 275°C (Tamme et al., 2010), and another sharp peak represents the solid-liquid phase change. It can be seen from the **table 4** that the phase change temperature of sodium nitrate is 306.9°C, the phase change temperature of the composites remained basically unchanged after adding nanoparticles, and after adding EG, the phase change temperature dropped by about 5°C. Wang (Wang et al., 2012) pointed out that the weak interaction between EG and binary eutectic nitrate, such as capillary force and surface tension, will cause a decrease in the phase change temperature.

According to reference (Wang et al., 2012), the theoretical latent heat of composites can be derived from **Formula (5)**.

$$\Delta H_{\text{theory}} = (1-\varphi)\Delta H_{\text{PCM}} \tag{5}$$

Where, ΔH_{theory} is the theoretical latent heat of the composites; φ is the mass fraction of EG and nanoparticles; ΔH_{PCM} is the latent heat of sodium nitrate. It can be seen from **Table 4** that the addition of nanoparticles has little effect on the latent heat of the composites, but when 15 wt% EG is added, the latent heat of the composites decreases greatly. This is because the addition of EG reduces the proportion of phase change materials in the composites, and EG keeps solid without phase change, so it has no contribution to the latent heat. On the other hand, the measured value of the latent heat of the composites is significantly lower than the theoretical value. The reason is that during the sintering process of the sample, some phase change material leakage is unavoidable. At the same time, Zhao (Zhao et al., 2016) and Feng (Feng et al., 2011) pointed out that the crystal arrangement and orientation of nitrate molecular chain would be limited by space effect and resistance due to the existence of insertion mechanism, which will lead to a decrease in the regularity of the crystal line region and an increase in lattice defects. As a result, compared with the theoretical value,

TABLE 4 | Phase change temperature and latent heat value of different samples.

Samples	Component	Phase change temperature/°C	Measurement of latent heat/(J/g)	Calculation value of latent heat/(J/g)	Measurement error
Sample 1	$NaNO_3$	306.9	178.8	-	-
Sample 2	$NaNO_3/SiO_2$	306.6	175.1	177.012	1.09%
Sample 3	$NaNO_3/(SiO_2+TiO_2)$	306.8	177.2	177.012	0.11%
Sample 4	$NaNO_3$/EG	301.9	150.1	151.98	1.25%
Sample 5	$NaNO_3/SiO_2$/EG	301.8	142.2	150.192	5.6%
Sample 6	$NaNO_3/(SiO_2+TiO_2)$/EG	301.9	147.8	150.192	1.62%

TABLE 5 | heat storage density of composite materials, Hitec salt and quaternary salt.

	$NaNO_3/(SiO_2+TiO_2)$/EG	Hitec salt	Ca $(NO_3)_2{\cdot}4H_2O$-KNO_3 - $NaNO_3$ -$NaNO_2$
specific heat before melting (J/(g·K))	1.81	—	—
specific heat after melting (J/(g·K))	2.47	1.4	1.52
onset melting point (°C)	301.9	142	84
termination melting point (°C)	312.8	146.7	169.2
heat of fusion (J/g)	147.8	80	80.28
Heat storage density (kJ/kg)	679.2	465.4	401

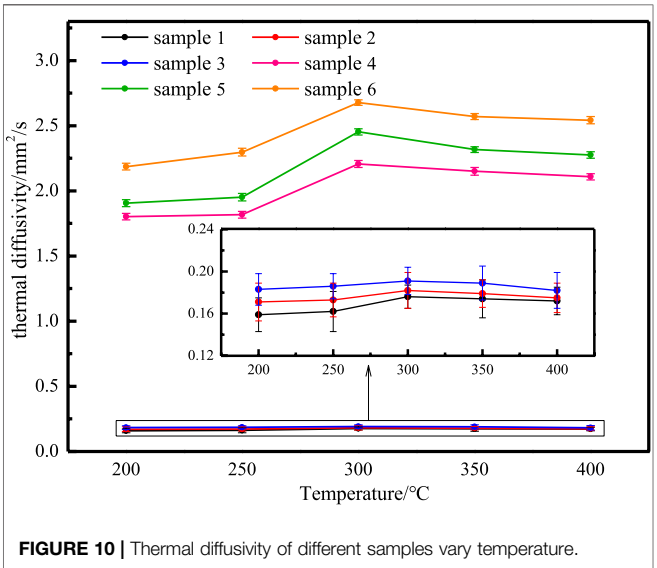

FIGURE 10 | Thermal diffusivity of different samples vary temperature.

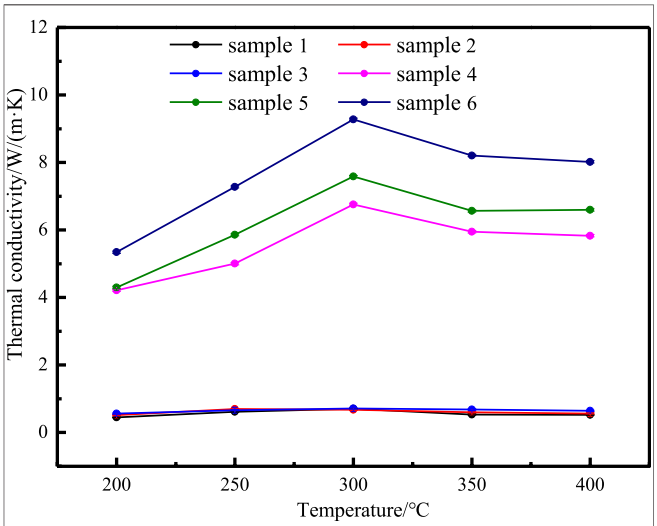

FIGURE 11 | Thermal conductivity of different samples vary temperature.

the latent heat of phase change of the composites will be reduced.

The decomposition temperature of industrial-grade $NaNO_3$ is 380°C, so the operating temperature should not exceed 380°C. Assuming that the working temperature range of the composite material is 100–380°C, the heat storage density of the composites can be calculated by **Formula (2)**. As shown in **Table 5**, the specific heat, fusion heat, melting point and other physical parameters of the composites studied in this paper and two commonly used low-melting mixed nitrates are listed. Using **Formula (2)**, the thermal storage density of $NaNO_3/(SiO_2+TiO_2)$/EG composites was 679.2 kJ/kg. In the temperature range of 100–380°C, the heat storage density of the commonly used low-melting Hitec salt is 465.4 kJ/kg, and the heat storage density of the mixed quaternary nitrate developed by this research group is 401 kJ/kg. It can be seen that although the addition of EG reduces the heat of fusion of sodium nitrate, because the specific heat capacity of the composite heat storage material increases, when the sensible heat and latent heat are used at the same time, the composite material still has a high heat storage density, and the heat storage density is much larger than two commonly used low melting point mixed nitrates.

TABLE 6 | Thermal diffusivity (mm^2/s) of different samples.

Temp-erature	Sample 1	Sample 2	Sample 3	Sample 4	Sample 5	Sample 6
200°C	0.159 (0.016)	0.171 (0.018)	0.183 (0.015)	1.803 (0.025)	1.906 (0.027)	2.186 (0.026)
250°C	0.162 (0.019)	0.173 (0.016)	0.186 (0.012)	1.817 (0.026)	1.952 (0.029)	2.297 (0.030)
300°C	0.176 (0.011)	0.182 (0.017)	0.191 (0.013)	2.207 (0.027)	2.453 (0.024)	2.687 (0.021)
350°C	0.174 (0.018)	0.179 (0.013)	0.189 (0.016)	2.15 (0.029)	2.317 (0.022)	2.570 (0.023)
400°C	0.172 (0.013)	0.175 (0.014)	0.182 (0.017)	2.108 (0.024)	2.276 (0.025)	2.542 (0.028)
Aver-age	0.1686	0.1760	0.1862	2.017	2.1808	2.4546

TABLE 7 | Thermal conductivity (W/(mK)) of different samples.

Temp-erature	Sample 1	Sample 2	Sample 3	Sample 4	Sample 5	Sample 6
200°C	0.446 (0.024)	0.519 (0.029)	0.559 (0.028)	4.213 (0.029)	4.293 (0.036)	5.342 (0.034)
250°C	0.613 (0.026)	0.699 (0.026)	0.660 (0.029)	5.00 (0.031)	5.858 (0.030)	7.277 (0.029)
300°C	0.702 (0.023)	0.672 (0.021)	0.709 (0.022)	6.758 (0.035)	7.583 (0.034)	9.279 (0.031)
350°C	0.535 (0.027)	0.599 (0.028)	0.681 (0.021)	5.948 (0.036)	6.565 (0.035)	8.208 (0.034)
400°C	0.523 (0.023)	0.564 (0.027)	0.643 (0.020)	5.832 (0.032)	6.596 (0.033)	8.019 (0.032)
Aver-age	0.55	0.61	0.65	5.55	6.18	7.63

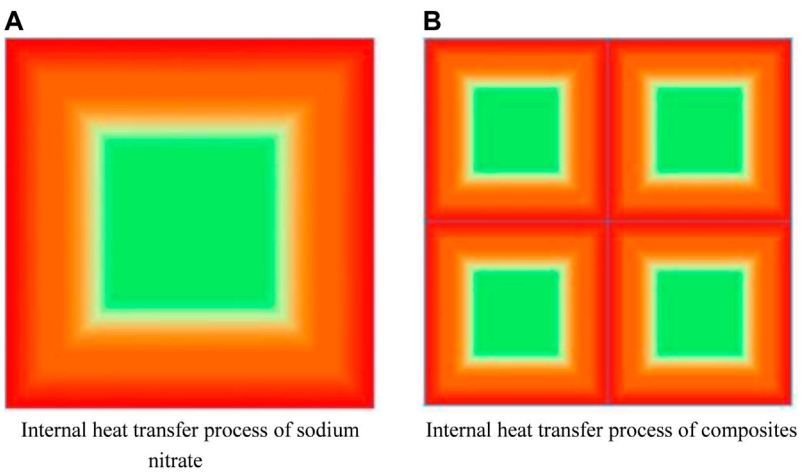

FIGURE 12 | Schematic diagram of the internal heat transfer process of different materials. **(A)** Internal heat transfer process of sodium nitrate. **(B)** Internal heat transfer process of composites.

Thermal Conductivity of Samples

Thermal conductivity is an important index to characterize the heat transfer rate of materials. The thermal diffusivity of different samples is measured in the temperature range of 200–400°C. **Figure 10** shows the thermal diffusivity of different samples vary with temperature. **Figure 11** shows the thermal conductivity of different samples vary with temperature. In the range of 200–400°C, the thermal diffusivity and thermal conductivity both first increases and then decreases with the increase in temperature, and the turning point is near the melting point. The measured thermal diffusivity and calculated thermal conductivity are listed in **Tables 6**, **7**. The results show that the addition of nanoparticles has a small increase in the thermal conductivity of $NaNO_3$, while the addition of EG can effectively increase the thermal conductivity of the composites sharply. At the same time, under the synergistic effect of nanoparticles and EG, the influence of improving the thermal conductivity is the best.

The addition of EG can improve the thermal conductivity of the composites, because it is evenly distributed in the composites, it forms an excellent heat transfer network. Heat can be quickly transferred to the inside of the nitrate along the mesh wall of EG, at the same time, EG itself has good thermal conductivity, and its own temperature quickly rises to a temperature close to the heating boundary. Therefore, in the subsequent heating process, nitrate is heated by multiple heating surfaces at the same time, the rate of heat transfer can increase exponentially. The schematic diagram of the heat transfer process is shown in **Figure 12**. On the other hand, after adding nanoparticles,

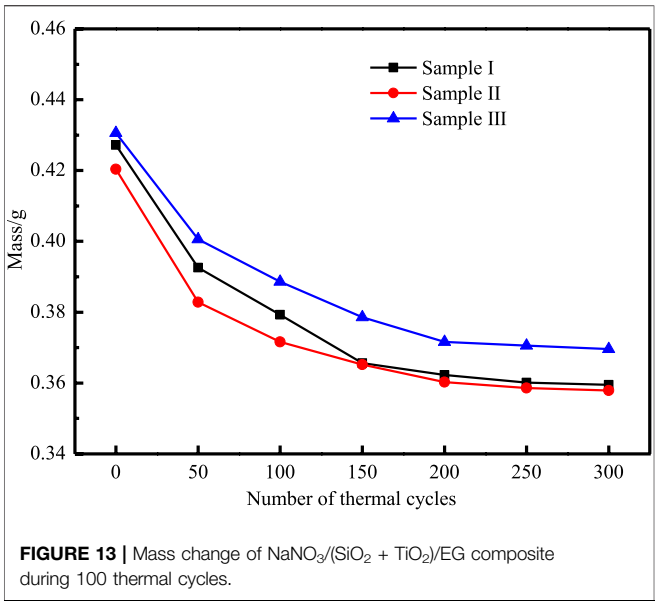

FIGURE 13 | Mass change of $NaNO_3/(SiO_2 + TiO_2)$/EG composite during 100 thermal cycles.

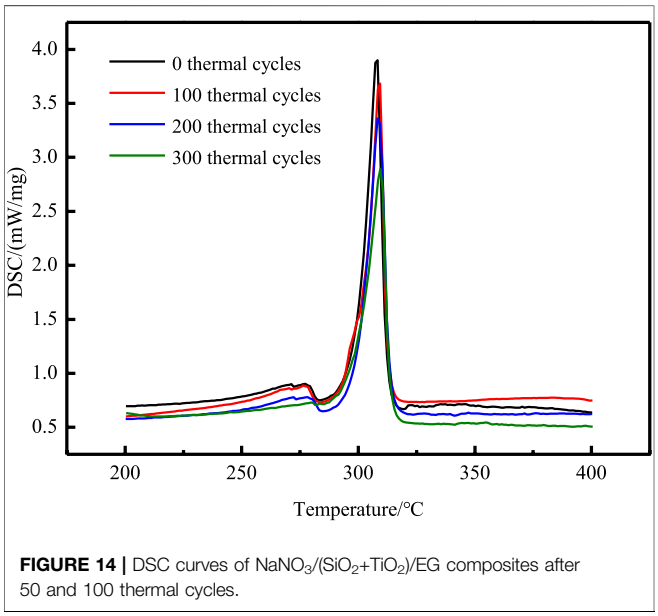

FIGURE 14 | DSC curves of $NaNO_3/(SiO_2+TiO_2)$/EG composites after 50 and 100 thermal cycles.

nanostructures similar to solids will be formed, and these nanostructures will form channels that facilitate heat transfer and increase the overall thermal conductivity of the composites.

Thermal Stability Test

The thermal cycling stability of the composites was analyzed by performing 300 heating-cooling thermal cycling experiments on three groups of samples in a muffle furnace. The mass change of the $NaNO_3/(SiO_2+TiO_2)$/EG composite during 300 thermal cycles is shown in **Figure 13**. The mass loss of composites is larger in the first 50 thermal cycles, changes less and less in the process of 50–150 thermal cycles, and shows a basically unchanged trend after 200 cycles. During the whole cycle, the mass loss rates of the three groups

TABLE 8 | Changes in phase change temperature and latent heat of composites during 100 thermal cycles.

Number of cycles	Phase change temperature/°C	Latent heat/J/g
0	301.9	147.8
100	301.6	142.9
200	301.5	138.7
300	301.7	136.9

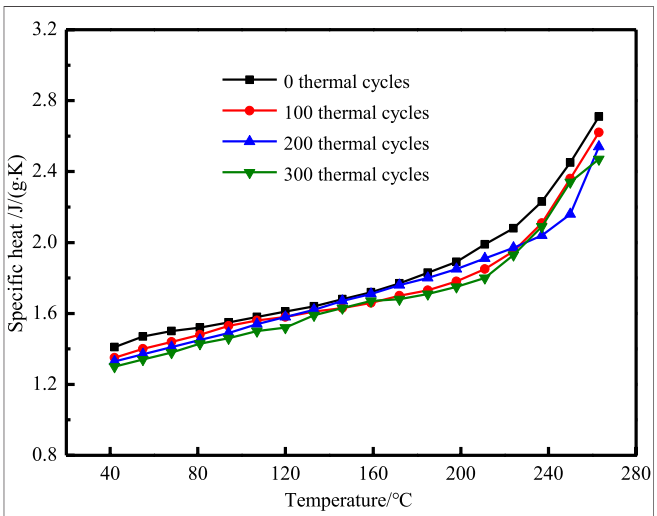

FIGURE 15 | Variation of specific heat after multiple thermal cycles (40–265°C).

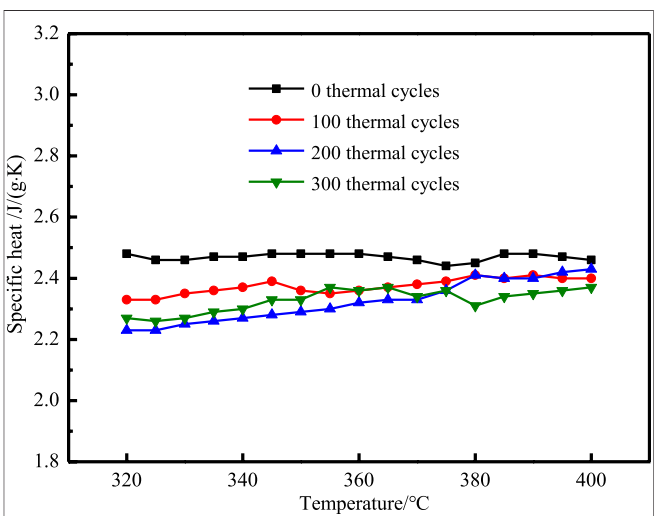

FIGURE 16 | Variation of specific heat after multiple thermal cycles (320–400°C).

of $NaNO_3/(SiO_2+TiO_2)$/EG composites were 15.9,14.9 and 14.2% respectively. The main reason is that a small amount of molten salt on the surface of the sample is easy to leak at high temperatures, but as the number of thermal cycles increases, after a small amount of sodium nitrate on the surface leaks, the inside is adsorbed by the

capillary force provided by the EG pores, and the mass changes little or basically remain unchanged, so as to ensure that it has a good thermal cycle and its stability.

Figure 14 show the DSC test curves of $NaNO_3/(SiO_2+TiO_2)$/EG composite after 300 heating cooling tests. The relevant physical parameters obtained from DSC curve analysis are listed in **Table 8**. It can be seen that during the cycle, the phase change temperature of the composites remained basically unchanged, and the decrease did not exceed 0.5°C. The latent heat of the $NaNO_3/(SiO_2+TiO_2)$/EG composites changed from 147.8 J/g to 136.9 J/g, a decrease of 7.4%, which indicating that the composites has good high temperature stability.

The specific heat of $NaNO_3/(SiO_2+TiO_2)$/EG composites after 300 heating cooling cycles are shown in **Figures 15**, **16**. It can be seen that after 100 thermal cycles, the specific heat began to decrease. The specific heat before phase change of $NaNO_3/(SiO_2+TiO_2)$/EG composites dropped from 1.81 J/(g·K) to 1.70 J/(g·K), a decrease of 6.1%, the specific heat after phase change of $NaNO_3/(SiO_2+TiO_2)$/EG composites dropped from 2.47 J/(g·K) to 2.32 J/(g·K), a decrease of 6.0%. In general, the composites have good stability when it is lower than 400°C.

CONCLUSION

Sodium nitrate/Nanoparticles/EG composites with stable shape were prepared by mechanical dispersion method. Sodium nitrate with different nanoparticles (1 wt%SiO_2, 0.9 wt%TiO_2+0.1 wt% SiO_2) were selected as phase change materials, and different mass fractions of EG (7, 10, 15, 20 wt%) were added. After screening out the best amount of EG added, the chemical compatibility, microstructure, specific heat, phase change temperature, latent heat, thermal conductivity and thermal cycle stability of the composites were studied. The main results are as follows:

1) During the preparation process of composites, nanoparticles, sodium nitrate and EG only have physical interactions and have good chemical compatibility. Sodium nitrate and nanoparticles can be uniformly dispersed in the pores of EG. When the EG content reaches 15 wt%, the shape of the composites is stable, and the mass loss rate before and after sintering is very small, which is 4.03%.
2) With the addition of EG and nanoparticles, the specific heat and thermal conductivity of the composites increase at the same time. The average specific heat before the phase change increased from 1.45 J/(g·K) to 1.81 J/(g·K), and the average specific heat after the phase change increased from 1.69 J/(g·K) to 2.47 J/(g·K). The thermal conductivity is increased to 7.63 w/(m·K), which is 13.9 times higher than that of sodium nitrate.
3) With the addition of nanoparticles, the phase change temperature and latent heat of the composites are basically unchanged. When 15 wt% EG is added, the phase change temperature of the composite drops by 5°C. In the range of 100–380°C, the heat storage density of the composite is about 679.2 kJ/kg.
4) After 300 heating-cooling cycles, the phase change temperature of the $NaNO_3/(SiO_2+TiO_2)$/EG composite does not change basically, the latent heat changed from 147.8 J/g to 136.9 J/g, a decrease of 7.4%, and the specific heat before and after the phase change is reduced by 6.1 and 6.0%, respectively. Therefore, the composites basically have good thermal stability.

DATA AVAILABILITY STATEMENT

The original contributions presented in the study are included in the article/Supplementary Material, further inquiries can be directed to the corresponding author.

AUTHOR CONTRIBUTIONS

All authors listed have made a substantial, direct, and intellectual contribution to the work and approved it for publication.

FUNDING

This work was supported by the National Natural Science Foundation of China (No. 52076006). and the National key research and development plan project (No. 2017YFB0903603).

REFERENCES

Acem, Z., Lopez, J., and Palomo Del Barrio, E. (2010). $KNO_3/NaNO_3$ - Graphite Materials for Thermal Energy Storage at High Temperature: Part I. - Elaboration Methods and Thermal Properties. *Appl. Therm. Eng.* 30 (13), 1580–1585. doi:10.1016/j.applthermaleng.2010.03.013

Andreu-Cabedo, P., Mondragon, R., Hernandez, L., Martinez-Cuenca, R., Cabedo, L., and Julia, J. E. (2014). Increment of Specific Heat Capacity of Solar Salt with SiO_2 Nanoparticles. *Nanoscale Res. Lett.* 9 (1), 582. doi:10.1186/1556-276x-9-582

Chieruzzi, M., Cerritelli, G. F., Miliozzi, A., and Kenny, J. M. (2013). Effect of Nanoparticles on Heat Capacity of Nanofluids Based on Molten Salts as PCM for Thermal Energy Storage. *Nanoscale Res. Lett.* 8 (1), 448. doi:10.1186/1556-276x-8-448

Da Cunha, J. P., and Eames, P. (2016). Thermal Energy Storage for Low and Medium Temperature Applications Using Phase Change Materials - A Review. *Appl. Energy* 177, 227–238. doi:10.1016/j.apenergy.2016.05.097

Farid, M. M., Khudhair, A. M., Razack, S. A. K, and Al- Hallaj, S. (2004). A Review on Phase Change Energy Storage: Materials and Applications. *Energy Convers. Manag.* 45 (9-10), 1597–1615. doi:10.1016/j.enconman.2003.09.015

Feng, L., Zhao, W., Zheng, J., Frisco, S., Song, P., and Li, X. (2011). The Shape-Stabilized Phase Change Materials Composed of Polyethylene Glycol and Various Mesoporous Matrices (AC, SBA-15 and MCM-41). *Sol. Energy Mater. Sol. Cells* 95, 3550–3556. doi:10.1016/j.solmat.2011.08.020

Fernández, A. G., Galleguillos, H., Fuentealba, E., and Pérez, F. J. (2015). Corrosion of Stainless Steels and Low-Cr Steel in Molten Ca $(NO_3)_2$–$NaNO_3$–KNO_3 Eutectic Salt for Direct Energy Storage in CSP Plants. *Sol. Energy Mater. Sol. Cells* 141, 7–13. doi:10.1016/j.solmat.2015.05.004

Gasia, J., Miró, L., and Cabeza, L. F. (2016). Review on System and Materials Requirements for High Temperature Thermal Energy Storage Part 1: General Requirements. *Renew. Sustain. Energy Rev.* 75, 1320. doi:10.1016/j.rser.2016.11.119

Gimenez, P., and Fereres, S. (2015). Effect of Heating Rates and Composition on the Thermal Decomposition of Nitrate Based Molten Salts. *Energy Procedia* 69, 654–662. doi:10.1016/j.egypro.2015.03.075

Ju, X., Xu, C., Hu, Y., Han, X., Wei, G., and Du, X. (2017). A Review on the Development of Photovoltaic/concentrated Solar Power (PV-CSP) Hybrid Systems. *Sol. Energy Mater. Sol. Cells* 161 (1), 305–327. doi:10.1016/j.solmat.2016.12.004

Kim, D., Jung, J., Kim, Y., Lee, M., Seo, J., and Khan, S. B. (2016). Structure and Thermal Properties of Octadecane/expanded Graphite Composites as Shape-Stabilized Phase Change Materials. *Int. J. Heat Mass Transf.* 95, 735–741. doi:10.1016/j.ijheatmasstransfer.2015.12.049

Li, Z., Sun, W. G., Wang, G., and Wu, Z. G. (2014). Experimental and Numerical Study on the Effective Thermal Conductivity of Paraffin/expanded Graphite Composite. *Sol. Energy Mater. Sol. Cells* 128, 447–455. doi:10.1016/j.solmat.2014.06.023

Li, R., Zhu, J., Zhou, W., Cheng, X., and Li, Y. (2016). Thermal Compatibility of Sodium Nitrate/Expanded Perlite Composite Phase Change Materials. *Appl. Therm. Eng.* 103, 452–458. doi:10.1016/j.applthermaleng.2016.03.108

Ling, Z., Chen, J., Xu, T., Fang, X., Gao, X., and Zhang, Z. (2015). Thermal Conductivity of an Organic Phase Change Material/expanded Graphite Composite across the Phase Change Temperature Range and a Novel Thermal Conductivity Model. *Energy Convers. Manag.* 102, 202–208. doi:10.1016/j.enconman.2014.11.040

Liu, R., Zhang, F., Su, W., Zhao, H., and Wang, C. a. (2015). Impregnation of Porous Mullite with Na_2SO_4 Phase Change Material for Thermal Energy Storage. *Sol. Energy Mater. Sol. Cells* 134, 268. doi:10.1016/j.solmat.2014.12.012

Liu, Z., Zhang, Y., Hu, K., Xiao, Y., Wang, J., Zhou, C., et al. (2016). Preparation and Properties of Polyethylene Glycol Based Semi-interpenetrating Polymer Network as Novel Form-Stable Phase Change Materials for Thermal Energy Storage. *Energy Build.* 127, 327–336. doi:10.1016/j.enbuild.2016.06.009

Lopez, J., Acem, Z., and Palomo Del Barrio, E. (2010). KNO3/NaNO3 - Graphite Materials for Thermal Energy Storage at High Temperature: Part II. - Phase Transition Properties. *Appl. Therm. Eng.* 30 (13), 1586–1593. doi:10.1016/j.applthermaleng.2010.03.014

Lu, M.-C., and Huang, C.-H. (2013). Specific Heat Capacity of Molten Salt-Based Alumina Nanofluid. *Nanoscale Res. Lett.* 8 (1), 292. doi:10.1186/1556-276x-8-292

Luo, Q., Liu, X., Wang, H., Xu, Q., Tian, Y., Liang, T., et al. (2022). Synergetic Enhancement of Heat Storage Density and Heat Transport Ability of Phase Change Materials Inlaid in 3D Hierarchical Ceramics. *Appl. Energy*, 306, 117995. doi:10.1016/j.apenergy.2021.117995

Madathil, P. K., Balagi, N., Saha, P., Bharali, J., Rao, P. V. C., Choudary, N. V., et al. (2016). Preparation and Characterization of Molten Salt Based Nanothermic Fluids with Enhanced Thermal Properties for Solar Thermal Applications. *Appl. Therm. Eng.* 109, 901–905. doi:10.1016/j.applthermaleng.2016.04.102

Mu, S., Guo, J., Yu, Y., An, Q., Zhang, S., Wang, D., et al. (2016). Synthesis and Thermal Properties of Cross-Linked Poly(acrylonitrile-Co-Itaconate)/polyethylene Glycol as Novel Form-Stable Change Material. *Energy Convers. Manag.* 110, 176–183. doi:10.1016/j.enconman.2015.12.004

Mu, S., Guo, J., Zhang, S., An, Q., Wang, D., Liu, Y., et al. (2016). Preparation and Thermal Properties of Cross-Linked Poly(acrylonitrile-Co-Itaconate)/polyethylene Glycol as Novel Form-Stable Phase Change Material for Thermal Energy Storage. *Mater. Lett.* 171, 23–26. doi:10.1016/j.matlet.2016.01.155

Qiao, X., Liu, X., Luo, Q., Song, Y., Wang, H., Chen, M., et al. (2021). Bifunctional Biomorphic SiC Ceramics Embedded Molten Salts for Ultrafast Thermal and Solar Energy Storage. *Mater. Today Energy* 21, 100764. doi:10.1016/j.mtener.2021.100764

Qin, Y., Leng, G., Yu, X., Cao, H., Qiao, G., Dai, Y., et al. (2015). Sodium Sulfate-Diatomite Composite Materials for High Temperature Thermal Energy Storage. *Powder Technol.* 282, 37–42. doi:10.1016/j.powtec.2014.08.075

Ren, Y., Xu, C., Yuan, M., Ye, F., Ju, X., and Du, X. (2018). $Ca(NO_3)_2$-$NaNO_3$/expanded Graphite Composite as a Novel Shape-Stable Phase Change Material for Mid- to High-Temperature Thermal Energy Storage. *Energy Convers. Manag.* 163, 50–58. doi:10.1016/j.enconman.2018.02.057

Shin, D., and Banerjee, D. (2011). Enhancement of Specific Heat Capacity of High-Temperature Silica-Nanofluids Synthesized in Alkali Chloride Salt Eutectics for Solar Thermal-Energy Storage Applications. *Int. J. Heat Mass Transf.* 54 (5–6), 1064–1070. doi:10.1016/j.ijheatmasstransfer.2010.11.017

Shin, D., and Banerjee, D. (2014). Specific Heat of Nanofluids Synthesized by Dispersing Alumina Nanoparticles in Alkali Salt Eutectic. *Int. J. Heat Mass Transf.* 74, 210–214. doi:10.1016/j.ijheatmasstransfer.2014.02.066

Song, M., Niu, F., Mao, N., Hu, Y., and Deng, S. (2018). Review on Building Energy Performance Improvement Using Phase Change Materials. *Energy Build.* 158 (1), 776–793. doi:10.1016/j.enbuild.2017.10.066

Song, W., Lu, Y., Wu, Y., and Ma, C. (2018). Effect of SiO_2 Nanoparticles on Specific Heat Capacity of Low-melting-point Eutectic Quaternary Nitrate Salt. *Sol. Energy Mater. Sol. Cells* 179, 66–71. doi:10.1016/j.solmat.2018.01.014

Tamme, R., Bauer, T., Buschle, J., Laing, D., Müller-Steinhagen, H., and Steinmann, W. D. (2010). Latent Heat Storage above 120°C for Applications in the Industrial Process Heat Sector and Solar Power Generation. *Int. J. Energy Res.* 32, 264–271. doi:10.1002/er.1346

Tao, Y. B., Lin, C. H., and He, Y. L. (2015). Preparation and Thermal Properties Characterization of Carbonate Salt/carbon Nanomaterial Composite Phase Change Material. *Energy Convers. Manag.* 97, 103–110. doi:10.1016/j.enconman.2015.03.051

Tao, Y., Mao, Z., Yang, Z., and Zhang, J. (2020). Preparation and Characterization of Polymer Matrix Passive Cooling Materials with Thermal Insulation and Solar Reflection Properties Based on Porous Structure. *Energy Build.* 225, 110361. doi:10.1016/j.enbuild.2020.110361

Tian, H., Wang, W., Ding, J., Wei, X., Song, M., and Yang, J. (2015). Thermal Conductivities and Characteristics of Ternary Eutectic Chloride/expanded Graphite Thermal Energy Storage Composites. *Appl. Energy* 148, 87. doi:10.1016/j.apenergy.2015.03.020

Tian, H., Wang, W., Ding, J., Wei, X., and Huang, C. (2016). Preparation of Binary Eutectic Chloride/expanded Graphite as High-Temperature Thermal Energy Storage Materials. *Sol. Energy Mater. Sol. Cells* 149, 187–194. doi:10.1016/j.solmat.2015.12.038

Tiznobaik, H., Banerjee, D., and Shin, D. (2015). Effect of Formation of "long Range" Secondary Dendritic Nanostructures in Molten Salt Nanofluids on the Values of Specific Heat Capacity. *Int. J. Heat Mass Transf.* 91, 342–346. doi:10.1016/j.ijheatmasstransfer.2015.05.072

Wang, W., Yang, X., Fang, Y., Ding, J., and Yan, J. (2009). Preparation and Thermal Properties of Polyethylene Glycol/Expanded Graphite Blends for Energy Storage. *Appl. Energy* 86 (9), 1479–1483. doi:10.1016/j.apenergy.2008.12.004

Wang, C., Feng, L., Li, W., Zheng, J., Tian, W., and Li, X. (2012). Shape-stabilized Phase Change Materials Based on Polyethylene Glycol/porous Carbon Composite: The Influence of the Pore Structure of the Carbon Materials. *Sol. Energy Mater. Sol. Cells* 105, 21–26. doi:10.1016/j.solmat.2012.05.031

Wei, H., Xie, X., Li, X., and Lin, X. (2016). Preparation and Characterization of Capric-Myristic-Stearic Acid Eutectic Mixture/modified Expanded Vermiculite Composite as a Form-Stable Phase Change Material. *Appl. energy* 178, 616–623. doi:10.1016/j.apenergy.2016.06.109

Wen, R., Huang, Z., Huang, Y., Zhang, X., Min, X., Fang, M., et al. (2016). Synthesis and Characterization of Lauric Acid/expanded Vermiculite as Form-Stabilized Thermal Energy Storage Materials. *Energy Build.* 116, 677–683. doi:10.1016/j.enbuild.2016.01.023

Xiao, J., Huang, J., Zhu, P., Wang, C., and Li, X. (2014). Preparation, Characterization and Thermal Properties of Binary Nitrate Salts/expanded Graphite as Composite Phase Change Material. *Thermochim. Acta* 587, 52–58. doi:10.1016/j.tca.2014.04.021

Yang, L. Z., Jiang, T., Li, G. H., Guo, Y. F., and Chen, F. (2018). Present Situation and Prospect of EAF Gas Waste Heat Utilization Technology. *High Temp. Mater. Process.* 37, 357–363. doi:10.1515/htmp-2016-0218

Yu, Q., Lu, Y., Zhang, C., Zhang, X., Wu, Y., and Sciacovelli, A. (2020). Preparation and Thermal Properties of Novel Eutectic Salt/nano-SiO2/Expanded Graphite Composite for Thermal Energy Storage. *Sol. Energy Mater. Sol. Cells* 215 (6), 110590. doi:10.1016/j.solmat.2020.110590

Yu, Q., Lu, Y., Zhang, X., Yang, Y., Zhang, C., and Wu, Y. (2021). Comprehensive Thermal Properties of Molten Salt Nanocomposite Materials Base on Mixed Nitrate Salts with SiO2/TiO2 Nanoparticles for Thermal Energy Storage. *Sol. Energy Mater. Sol. Cells* 230 (2), 111215. doi:10.1016/j.solmat.2021.111215

Zalba, B., Marı´n, J. M., Cabeza, L. F., and Mehling, H. (2003). Review on Thermal Energy Storage with Phase Change: Materials, Heat Transfer Analysis and Applications. *Appl. Therm. Eng.* 23 (3), 251–283. doi:10.1016/s1359-4311(02)00192-8

Zhang, Q., Wang, H., Ling, Z., Fang, X., and Zhang, Z. (2015). RT100/expand Graphite Composite Phase Change Material with Excellent Structure Stability, Photo-Thermal Performance and Good Thermal Reliability. *Sol. Energy Mater. Sol. Cells* 140, 158–166. doi:10.1016/j.solmat.2015.04.008

Zhao, T., She, S., Ji, X., Guo, X., Jin, W., Zhu, R., et al. (2016). Expanded Graphite Embedded with Aluminum Nanoparticles as Superior Thermal Conductivity Anodes for High-Performance Lithium-Ion Batteries. *Sci. Rep.* 6, 33833. doi:10.1038/srep33833

Zhong, L., Zhang, X., Luan, Y., Wang, G., Feng, Y., and Feng, D. (2014). Preparation and Thermal Properties of Porous Heterogeneous Composite Phase Change Materials Based on Molten Salts/expanded Graphite. *Sol. Energy* 107, 63–73. doi:10.1016/j.solener.2014.05.019

Zhuo, L., and Wu, Z. G. (2014). Numerical Study on the Thermal Behavior of Phase Change Materials (PCMs) Embedded in Porous Metal Matrix. *Sol. Energy* 99, 172–184. doi:10.1016/j.solener.2013.11.017

Conflict of Interest: The authors declare that the research was conducted in the absence of any commercial or financial relationships that could be construed as a potential conflict of interest.